PCCP

PAPER

View Article Online
View Journal | View Issue

Cite this: *Phys. Chem. Chem. Phys.*, 2025, **27**, 16067

Metastable-phase crystallization of potassium acetate triggered by focused irradiation with ultrashort laser pulses†

Hozumi Takahashi * and Hiroshi Y. Yoshikawa *

Received 17th April 2025,
Accepted 8th July 2025

DOI: 10.1039/d5cp01478f

rsc.li/pccp

The preparation of desired crystal polymorphs has significant implications for designing materials with tailored properties; however, conventional methods often face limitations in terms of precision and reproduction. In this study, we demonstrate the crystallization of a metastable phase of potassium acetate by ultrashort laser ablation of supersaturated aqueous solutions. By varying the laser energy (0.1–300 μJ per pulse) and pulse duration (0.1–10 ps), we found that shorter laser pulses could induce metastable-phase crystallization with lower pulse energy. We also systematically investigated cavitation bubble generation, which is a possible perturbation of crystallization, revealing that shorter laser pulses can provide a higher crystallization probability even with smaller cavitation bubbles. Our results suggest that the precise regulation of positive (*e.g.*, cavitation bubble generation) and negative effects (*e.g.*, temperature elevation) is crucial for the induction of metastable-phase crystallization, which has potential applications in pharmaceuticals, advanced materials, and chemical engineering.

Introduction

Crystal polymorphism, the ability of a compound to exist in multiple crystalline forms, has attracted considerable attention in diverse scientific and industrial fields, because it significantly influences the physical and chemical properties of materials, such as stability, solubility, and bioavailability.[1–5] Therefore, the precise manipulation of crystal polymorphs has significant implications for designing materials with tailored properties. Despite progress in conventional crystallization methods, the precise and reproducible production of desired polymorphs remains challenging,[6] especially for metastable phases that often transiently transform into more thermodynamically stable phases.

Laser-induced crystallization has recently emerged as a powerful approach to address the challenges in controlling crystallization in a spatial and temporal manner.[7–9] For instance, non-photochemical laser-induced nucleation (NPLIN), where unfocused irradiation with nanosecond to picosecond laser pulses into supersaturated solutions or supercooled melts induces crystal nucleation,[7,10,11] has demonstrated the control of crystal polymorphs for amino acids and pharmaceuticals by varying laser parameters such as the laser power and polarization mode.[12–15] In addition, optical trapping-induced crystallization (OTIC), where condensation of solutes induced *via* optical pressure with a tightly focused laser beam results in crystal nucleation,[8,16–18] has exhibited not only polymorphic selectivity[19–23] but also enantioselectivity[24–30] by precisely adjusting laser parameters together with solution conditions (*e.g.*, concentration, additives). In these techniques, the physical effects of laser irradiation, including electric field and/or heat generation, serve as localized and transient perturbations that trigger crystallization.

As another laser-induced crystallization technique that mainly utilizes the photophysical effects of laser irradiation, laser ablation, macroscopic morphological change in materials induced by laser irradiation above a certain energy threshold, has exhibited promise for precise control of crystallization (*e.g.* crystal nucleation, crystal growth, polymorphic transition).[31–42] In particular, laser ablation of solutions yields metastable phases of various compounds including pharmaceutics such as indomethacin and aspirin,[43–46] which can potentially exhibit better bioavailability due to higher solubility.[47] As for the mechanism of crystal nucleation, previous studies have underscored the pivotal role of cavitation bubbles, which expand, shrink, and collapse in microseconds, by increasing the local concentration and/or decreasing the interfacial energy at cavitation bubble surfaces.[9,31,37,39,48–54] However, laser-induced cavitation bubble behaviors that affect metastable-phase crystallization have not clearly been understood. Thus, further

Graduate School of Engineering, The University of Osaka, 2-1, Yamada-oka, Suita, Osaka 565-0871, Japan. E-mail: h.takahashi@eei.eng.osaka-u.ac.jp, hiroshi@ap.eng.osaka-u.ac.jp

† Electronic supplementary information (ESI) available. See DOI: https://doi.org/10.1039/d5cp01478f

investigation of the correlation between cavitation bubbles and crystallization behavior is crucial for harnessing the full potential of laser ablation-driven crystallization in both fundamental and applied contexts.

This study systematically explored the role of cavitation bubble behavior with various laser parameters in crystallizing metastable phases. We used potassium acetate (CH_3COOK, denoted as AcOK) as a target compound, which exhibits several pseudo-polymorphs upon crystallization from aqueous solution, including AcOK·$0H_2O$ (anhydrate phase), AcOK·xH_2O (x = 0.38–0.44), 3AcOK·$2H_2O$, and AcOK·$2H_2O$.[55] Furthermore, AcOK can be easily crystallized from aqueous solutions by applying external stimuli, which may facilitate the *in situ* monitoring of crystallization induced with a single laser pulse. In this study, ultrashort laser pulses were focused into supersaturated AcOK aqueous solution by systematically screening laser energy and pulse duration across a range of 0.1–300 μJ per pulse and 0.1–10 ps, respectively. We also investigated the behavior of cavitation bubbles under these laser conditions to understand the underlying mechanism of crystallization of the metastable phase by laser ablation. These results offer a pathway toward precise polymorphic control using ultrashort laser ablation, with implications for pharmaceutical manufacturing, advanced material design, and chemical engineering.

Experimental protocols

Sample preparation

Anhydrous potassium acetate (AcOK·$0H_2O$) purchased from Wako (≥97%) was employed without further purification. First, large amounts of AcOK aqueous solutions with a molality (m) of 32.6 or 33.9 mol kg^{-1} were prepared by completely dissolving the reagent powders in pure water (18.2 MΩ cm) at ∼80 °C using a heat bath. Then, 1-mL aliquots of the solutions were dispensed into glass vials (S-7, Nichiden-Rika) while warming. Subsequently, the solution was incubated at room temperature (∼22 °C) for more than 20 min. The solution temperature over incubation time was measured using thermography (SGT, AS ONE). It decreased over the incubation time and became comparable to that at room temperature approximately 20-min after incubation (Fig. S1, ESI†). After incubation, the glass vial containing the solution was mounted on an inverted microscope (IX71, Olympus) and used for subsequent laser experiments.

Optical setup for laser-induced experiments

The optical setup for the laser-induced crystallization is illustrated in Fig. S2a (ESI†). A regeneratively amplified Ti:Sapphire laser system (Astrella, Coherent) was used as the light source for laser ablation. The central wavelength was set at 800 nm. Because the AcOK aqueous solution has significantly lower absorbance at 800 nm (Fig. S3, ESI†), it is reasonable to assume that electron excitation by single-photon absorption does not take place upon exposure to an 800 nm-laser, indicating that multiphoton excitation was essentially involved in laser ablation of the solution in this study. The pulse duration was adjusted to 0.1, 0.5, 1, 5, and 10 ps by adjusting the angle of the grating within the stretcher of the chirped amplified laser system. The laser energy was controlled using a combination of a half-wave plate (WPH10M-808, Thorlabs) and a polarizing beam splitter (GL15-B, Thorlabs). The laser pulses were introduced into the microscope and focused onto the sample solution using an objective lens (10×, NA = 0.30, UPLFLN10X2, Olympus). The focal radius is estimated to be ∼1.6 μm by Rayleigh's criterion (0.61 × λ/NA). Accordingly, the laser fluence corresponding to the energy regime of 0.1–300 μJ is calculated to be 1.2–3600 J cm^{-2}. The laser focus was set approximately 5 mm above the bottom of the glass vial. The macroscopic behavior was observed from the side of the glass vial using a camera (iPhone 12 mini, Apple), whereas microscopic behavior through the objective lens was captured using a CMOS camera (WRAYCAM-CIX832, WRAYMER).

Fig. S2b (ESI†) shows the optical setup for observing the laser-induced cavitation bubbles. In contrast to the laser-induced crystallization experiments, laser pulses were introduced into the sample solution in the horizontal direction through an objective lens (10×, NA = 0.30, UPLFLN10X2, Olympus). Microscopic images of cavitation bubble generation were captured with a high-speed camera (HPV-2, Shimadzu, 1 000 000 frames per s) through a microscope (objective lens: 10×, NA = 0.25, LMPLFLN10X, Olympus). The ImageJ software (NIS) was used for image analysis and contrast adjustment.

Results and discussion

Crystallization behavior without laser irradiation

Prior to the laser experiments, we initially clarify which pseudo-polymorphs of AcOK crystals could be obtained from aqueous solutions by spontaneously crystallizing them without laser exposure. In the case of AcOK solution with m = 33.9 mol kg^{-1}, as soon as the solution was transferred from the heat bath (∼80 °C) to ambient conditions (∼22 °C), needle-like crystals were formed in the entire solution. Fig. S4a and Movie S1 (ESI†) show the microscopic crystallization behavior of AcOK in a solution with m = 33.9 mol kg^{-1}. Needle-like crystals initially grew in the solution (t = 0–90 min). After approximately 2 h of incubation, plate-like crystals appeared, and needle-like crystals started to dissolve (t = 120 min). Notably, the needle-like crystals were converted into fragments of plate-like crystals (t = 165–180 min). We also confirmed that the plate-like crystals showed no birefringence, while the needle-like crystals exhibited birefringence (Fig. S4b, ESI†). Furthermore, we found that the plate-like crystals and needle-like crystals showed distinct Raman spectra at ∼1400 cm^{-1} (Fig. S5, ESI†). These results indicate that needle-like crystals were metastable phase, whereas the plate-like crystals were stable phase. Indeed, Kalle *et al.* have recently reported the following results: (1) only the crystals of AcOK·xH_2O do not show birefringence among the pseudo-polymorphs, (2) the transformation (hydration) of AcOK·$0H_2O$ into AcOK·xH_2O and 3AcOK·$2H_2O$ can take place at room temperature, and (3) 3AcOK·$2H_2O$ is more stable than AcOK·xH_2O.[55] Accordingly, we considered that the

stable and metastable phases observed in this study may correspond to AcOK·xH$_2$O and AcOK·0H$_2$O, respectively.

We also observed the crystallization behavior of a solution with a lower concentration, m = 32.6 mol kg^{-1}. Prolonged incubation resulted in spontaneous crystallization of the stable phase. Fig. S6 (ESI†) shows the spontaneous crystallization probability as a function of time. The crystallization probability is defined as the ratio of the number of crystallized samples to the total number of prepared samples. The spontaneous crystallization probability increased with increasing incubation time. Specifically, crystallization was rarely observed after 20 min of incubation (3.3%, 1/30). Then, crystallization was observed in 40% (12/30) of the samples after 40 min, increased to 93% (28/30) after 80 min. According to the temporal evolution of the solution temperature (Fig. S1, ESI†) and spontaneous crystallization probability (Fig. S6, ESI†), subsequent crystallization experiments were conducted using a 32.6 mol kg^{-1} AcOK aqueous solution incubated for 20–25 min to avoid spontaneous crystallization before laser irradiation.

Crystallization behavior of AcOK by laser irradiation

Fig. 1a and Movie S2 (ESI†) show the macroscopic behavior of AcOK crystallization induced by a 0.1-ps laser pulse with energy (E) of 60 μJ per pulse. After a single shot, needle-like crystals formed around the laser focus. These grew radially from the laser focus over time. To observe the crystallization behavior in detail, microscopic imaging was performed (Fig. 1b and Movie S3, ESI†). After a single shot, bubbles formed around the laser focus ($t \sim 0$ s). These bubbles may correspond to gas bubbles, probably originating from the dissolved gas and/or photochemical products of the solution.[57] Then, needle-like crystals appeared around the bubbles and gradually grew. During this process, plate-like crystals (stable phase), as shown in Fig. S4 (ESI†), were not observed around the laser-induced bubbles. These results indicate that the laser ablation of the solution can provide a metastable phase of AcOK.

Previous studies on laser ablation-induced crystallization have indicated that the laser parameters (*e.g.*, laser energy, pulse duration, repetition rate, and wavelength) significantly influence the efficiency of crystallization by laser irradiation,[9,37,39,40,44,46,49,54,58,59] whereas the impact of the laser parameters on metastable-phase crystallization is less understood. Accordingly, in this study, we systematically investigated the dependence of the crystallization of the metastable phase of AcOK on the laser energy and pulse duration. Fig. 2a shows the crystallization probability for the 0.1-, 0.5- and 1-ps laser pulses as a function of the laser energy (the raw data are summarized in Table S1, ESI†). For each pulse duration, the crystallization probability monotonically increased with laser energy and finally reached 100%. The threshold energy for inducing crystal nucleation increased with pulse duration: 5 μJ per pulse for the 0.1-ps laser pulse, 10 μJ per pulse for the 0.5-ps laser pulse, and 22 μJ per pulse for the 1-ps laser pulse. Similarly, the laser energy required to achieve 100% crystallization probability also tended to increase with pulse duration, from 10 μJ per pulse for the 0.1-ps laser pulse to 45 μJ per pulse for the 0.5-ps and 1-ps laser pulse. On the other hand, Fig. 2b shows the crystallization probability for the 5-ps and 10-ps laser pulses (see also Table S1, ESI†). In contrast to the 0.1-, 0.5- and 1-ps laser pulses, the crystallization probability did not increase monotonically. Specifically, it initially increased with the laser energy but

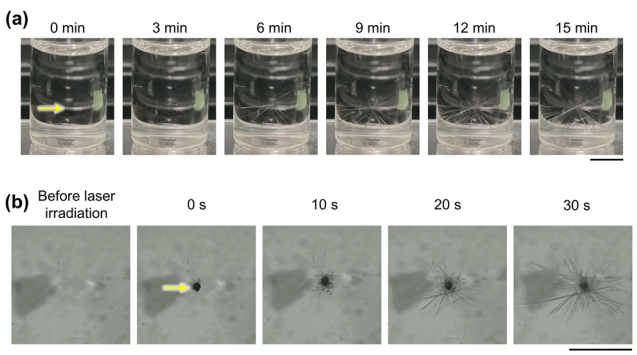

Fig. 1 (a) Macroscopic and (b) microscopic images of the crystallization behavior of AcOK triggered by a single 0.1-ps laser pulse with E = 60 μJ per pulse. The yellow arrows indicate the laser focus. The time upon laser irradiation was defined as t = 0 min and 0 s. Scale bars: (a) 5 mm, (b) 0.5 mm.

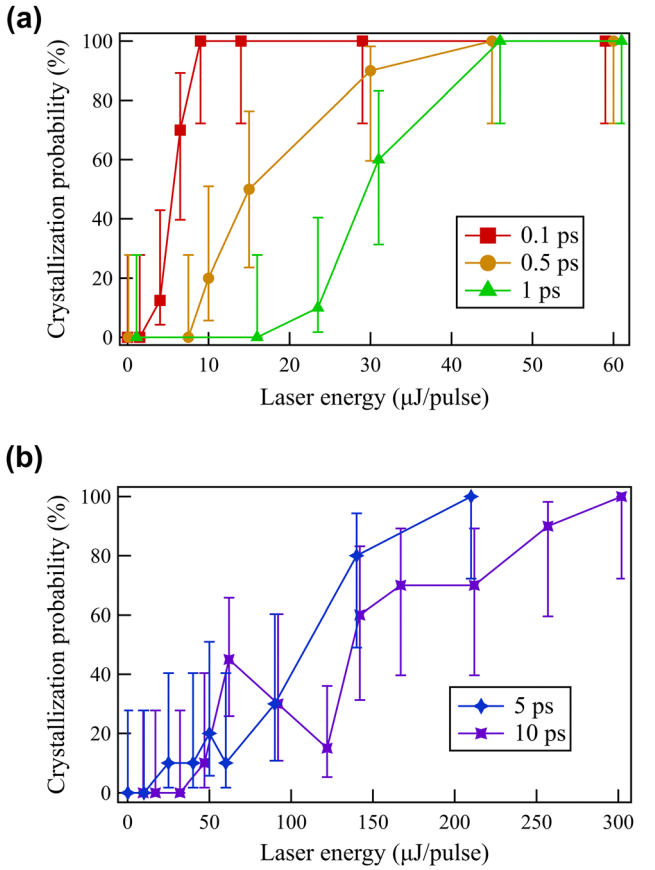

Fig. 2 Dependence of laser energy on crystallization probability for the (a) 0.1-ps, 0.5-ps, and 1-ps laser pulses and (b) 5-ps and 10-ps laser pulses. At least ten samples were tested under each condition. The error bars represent the confidence intervals that were calculated by the Wilson method for the binomial distribution.[56]

then decreased. In particular, we found that the difference in crystallization probability for the 10-ps laser pulse at 60 μJ per pulse (crystallization probability: 45%) *vs.* 120 μJ per pulse (15%) is statistically significant under the chi-squared test [$\chi^2(1) = 4.3$, $P = 3.8\%$]. It should be mentioned that such a decrease in crystallization probability above a certain laser energy has been reported for white hen egg lysozyme solution, glacial acetic acid melt, and sodium acetate solution.[37,40,49] After decreasing once, the crystallization probability increased again and finally reached 100% at 210 μJ per pulse for the 5-ps laser pulse and 300 μJ per pulse for the 10-ps laser pulse. This result indicated that laser irradiation exerted both positive and negative effects on AcOK crystallization. The threshold energies for inducing crystal nucleation for the 5-ps ($\sim$25 μJ per pulse) and 10-ps laser pulse ($\sim$45 μJ per pulse) were seemingly larger than those for the 0.1-, 0.5-, and 1-ps laser pulse ($\leq \sim$22 μJ per pulse). These results indicate that shorter laser pulses can more effectively provide a metastable phase of AcOK crystals.

Dependence of cavitation bubble generation on laser energy and pulse duration

Thus far, the significance of cavitation bubble generation in the formation of metastable phase crystals has been emphasized not only in the study of laser ablation-induced crystallization,[40,44,46] but also in other studies such as ultrasound-induced[60–62] and mechanical shock-induced crystallization.[63] We also confirmed that the metastable phase of AcOK could be prepared by applying mechanical shock (Fig. S7a and Movie S4, ESI†) and ultrasound (Fig. S7b and Movie S5, ESI†). These results suggest that cavitation bubble generation plays a crucial role in the formation of the metastable phase of the AcOK crystals. Therefore, we conducted a systematic investigation of laser-induced cavitation bubbles to understand the influence of laser parameters on the crystallization of the metastable phase. Movie S6 (ESI†) shows the behavior of the cavitation bubble induced by a single laser pulse with different laser energies (E = 2–60 μJ per pulse) and pulse durations (Δt = 0.1–10 ps). As representative examples, Fig. 3 and 4 show the behavior of cavitation bubbles generated by focused irradiation with 0.1- to 10-ps laser pulse with E = 10 μJ per pulse and 60 μJ per pulse, respectively. The temporal evolution of length of the cavitation bubbles determined from Fig. 3a and 4a is shown in Fig. 3b (E = 10 μJ per pulse) and Fig. 4b (E = 60 μJ per pulse), while that of the width is shown in Fig. 3c (E = 10 μJ per pulse) and Fig. 4c (E = 60 μJ per pulse). The length and width of the cavitation bubbles were defined as the sizes along the axial direction and perpendicular to the axis, respectively. In all cases, the cavitation bubbles expanded, shrank, and finally collapsed at the microsecond timescale. Herein, we describe the detailed behavior of cavitation bubble generation by considering the case of a 1-ps laser pulse as an example (Fig. 3a, middle). Upon laser irradiation, a cavitation bubble elongating along the axial direction was formed (t = 1 μs). Such an elongated bubble morphology was well observed in ultrashort laser pulse irradiation, known as laser-induced filamentation.[64,65] Both the length and width of the cavitation bubble initially expanded and reached their maximum size at 4–6 μs (270 μm) and 10–13 μs (160 μm), respectively. Subsequently, they began to shrink and exhibited re-expansion and re-shrinking motions several times. After the collapse of the cavitation bubble, small bubbles appeared, probably owing to the long-lasting bubble observed in Fig. 1b. As the pulse duration dependence, we found that the elongated shape of cavitation bubbles at the early time phase (t = 1 μs) *via* laser-induced filamentation was more prominent by the laser irradiation with shorter pulse duration. The cavitation bubbles generated by laser pulse with higher energy, E = 60 μJ per pulse, showed an approximately similar expansion, shrinkage, and collapsing motions, while the maximum size and collapsing timing increased (Fig. 4).

Fig. 5a and b show the dependence of the maximum length and width of the cavitation bubbles on the laser energy and pulse duration. Both the maximum length and width monotonically increased with the laser energy. As with the previous studies,[37,39,40,49,54] the trend was well-fitted with a logarithmic function, $k\ln(E/E_{th})$, where k models the rate of increase and E_{th} is the threshold energy for cavitation bubble generation (k and E_{th} are summarized in Table S2, ESI†). Regarding the impact of the pulse duration, in the case of the maximum length (Fig. 5a), shorter laser pulses tended to provide longer cavitation bubbles in this energy window. This is possibly because shorter laser pulses can enhance the laser-induced filamentation.[66] By contrast, the order of the maximum width of cavitation bubbles (Fig. 5b) changed in a different manner, especially at the relatively lower laser energy regime (*e.g.*, $E \leq$ 20 μJ per pulse). For instance, at E = 5 μJ per pulse, the order was 10 ps < 5 ps < 0.1 ps < 1 ps < 0.5 ps. At E = 15 μJ per pulse, it changed completely to 0.1 ps < 10 ps < 0.5 ps < 5 ps < 1 ps. At even higher energy regimes (*e.g.*, $E \geq$ 45 μJ per pulse), the order approximately followed the order of pulse duration: 0.1 ps < 0.5 ps < 1 ps < 10 ps < 5 ps. We found that both the threshold energy for cavitation bubble generation (E_{th}) and the rate of increase (k) tended to increase with pulse duration (Table S2, ESI†). As for E_{th}, the average threshold energies derived from the fitting curves of maximum length and width were 0.68 μJ per pulse for the 0.1-ps laser pulse, 1.1 μJ per pulse for the 0.5-ps laser pulse, 1.5 μJ per pulse for the 1-ps laser pulse, 3.2 μJ per pulse for the 5-ps laser pulse, and 4.7 μJ per pulse for the 10-ps laser pulse. This trend can be attributed to the difference in the peak power density of the laser pulses; shorter laser pulses should facilitate the induction of multiphoton excitation, which is the initial step in laser ablation. On the other hand, the rate of increase (k) of the bubble length was 111 μm for the 0.1- and 0.5-ps laser pulses, 121 μm for the 1-ps laser pulse, 158 μm for the 5-ps laser pulse, and 176 μm for the 10-ps laser pulse, while that for bubble width was 49 μm for the 0.1-ps laser pulse, 81 μm for the 0.5-ps laser pulse, 98 μm for the 1-ps laser pulse, 136 μm for the 5-ps laser pulse, and 150 μm for the 10-ps laser pulse. This result implies that a prolonged energy input with a longer laser pulse allows larger energy absorption for molecules and/or a larger percentage of the absorbed energy transforms for cavitation bubble generation for longer pulse durations. In fact, it has been reported that the generation of cavitation bubbles in water can be sensitively altered with pulse

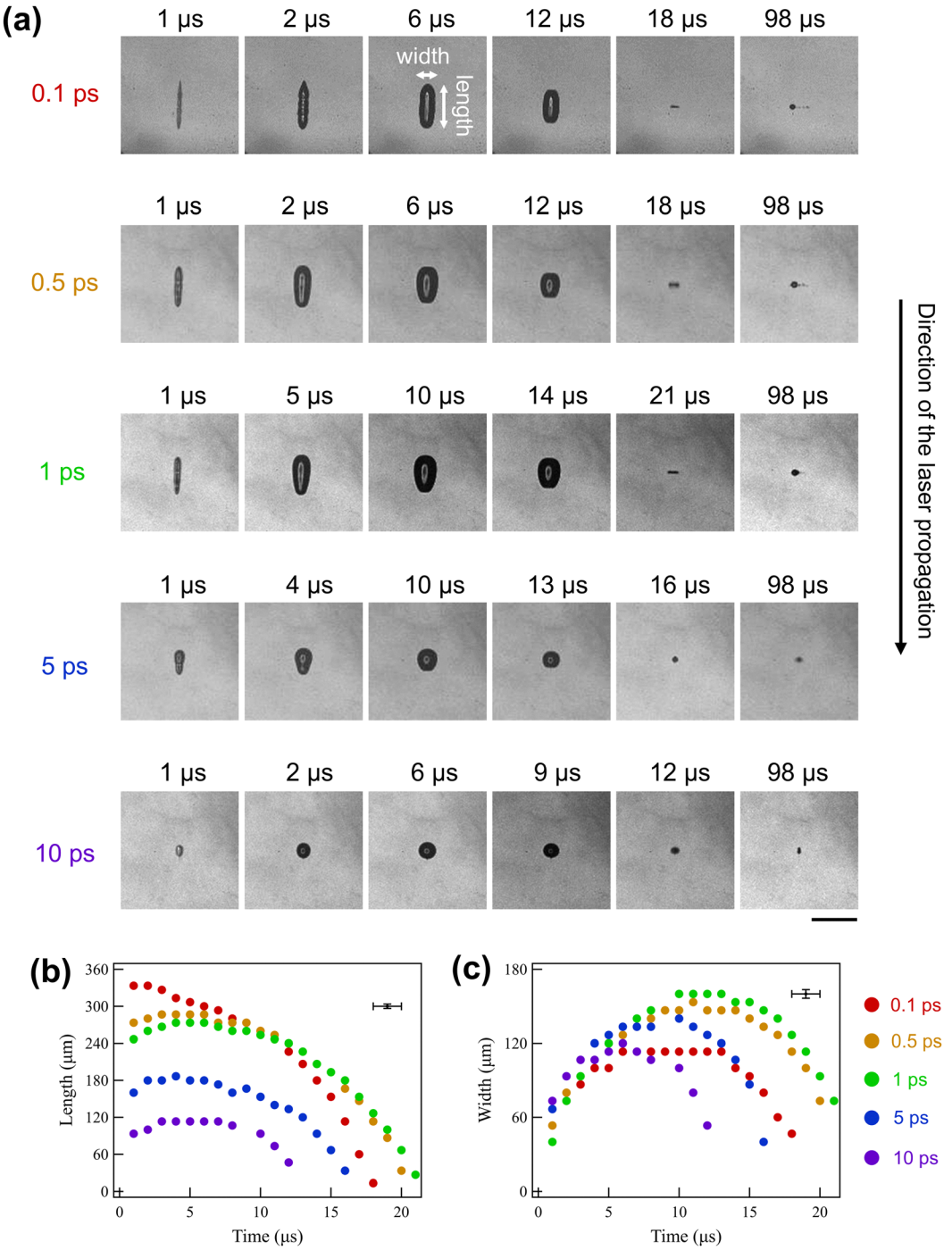

Fig. 3 (a) Behavior of cavitation bubble generation induced by a 0.1–10-ps laser pulse with E = 10 μJ per pulse. To avoid crystallization upon laser irradiation, AcOK aqueous solution with m = 20.9 mol kg^{-1}, which is 36% lower than that of the solution used in the laser experiments, was employed. Scale bar: 300 μm. Temporal evolution of (b) length and (c) width of the cavitation bubble. The size of the cavitation bubble was plotted until the first maximum shrinkage of it. Uncertainties in the upper right represent a single-frame exposure time (1 μs) and a single pixel (7 μm).

duration.[66,67] Accordingly, the overall tendency of the cavitation bubble size with pulse duration can be qualitatively explained as follows: shorter laser pulses provide larger cavitation bubbles in the lower-energy regime because of lower E_{th}, whereas longer laser pulses eventually provide larger cavitation bubbles in the higher-energy regime as larger k becomes more significant.

Discussion

Several previous studies of laser ablation-induced crystallization have reported that the generation of cavitation bubbles plays a pivotal role in inducing crystallization by locally increasing solute concentrations, enhancing heterogeneous nucleation, *etc.*[9,31,37,39,40,46,49–54] For instance, our previous demonstration

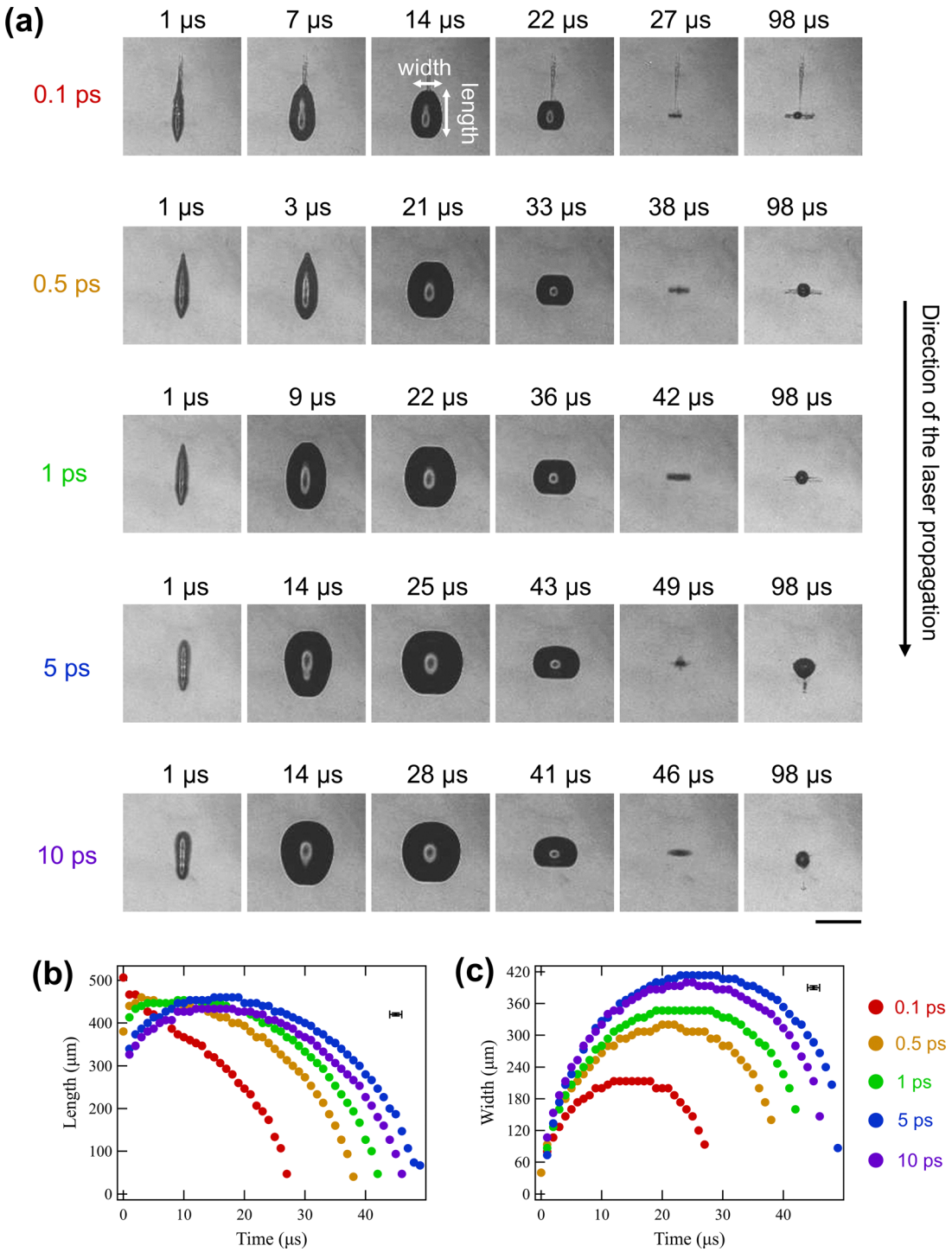

Fig. 4 (a) Behavior of cavitation bubble generation induced by a 0.1–10-ps laser pulse with E = 60 μJ per pulse. To avoid crystallization upon laser irradiation, AcOK aqueous solution with m = 20.9 mol kg^{-1}, which is 36% lower than that of the solution used in the laser experiments, was employed. Scale bar: 300 μm. Temporal evolution of (b) length and (c) width of the cavitation bubble. The size of the cavitation bubble was plotted until the first maximum shrinkage of it. Uncertainties in the upper right represent a single-frame exposure time (1 μs) and a single pixel (7 μm).

of ice crystallization revealed that the size of the cavitation bubble and crystallization probability are correlated: larger cavitation bubbles tend to provide a higher crystallization probability.[39] In addition, recent theoretical studies revealed the concentration dynamics achieved at the cavitation bubble surface and found that larger cavitation bubbles potentially provide a higher concentration due to the faster bubble growth velocity.[9,53]

Accordingly, we now discuss the impact of laser parameters on the crystallization of the metastable phase of AcOK from the

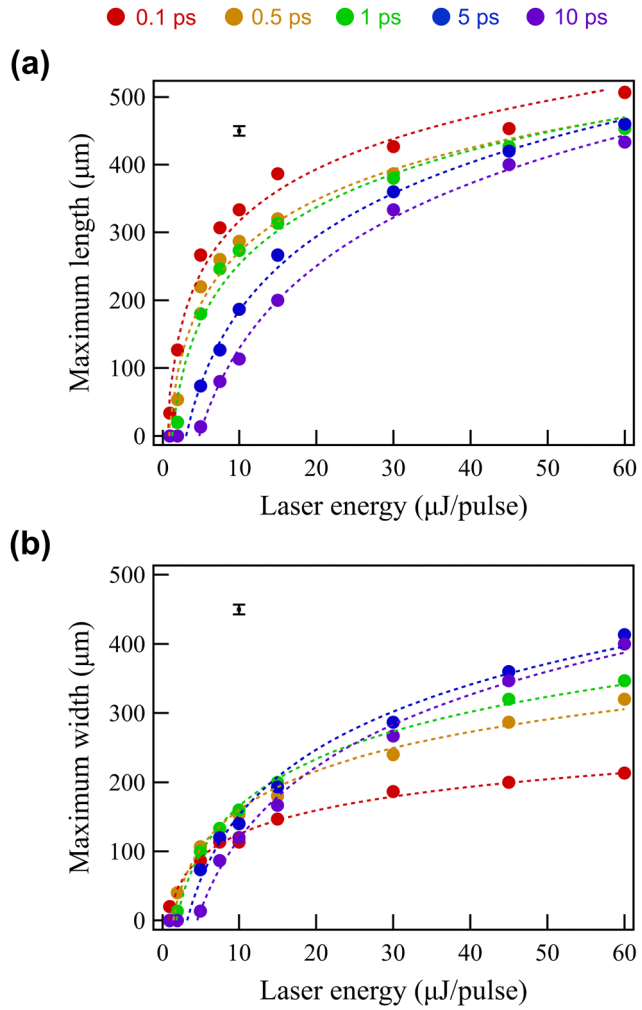

Fig. 5 Dependence of the maximum (a) length and (b) width of cavitation bubble on laser energy and pulse duration. The error bars represent uncertainties in the scale of 1 pixel (7 μm).

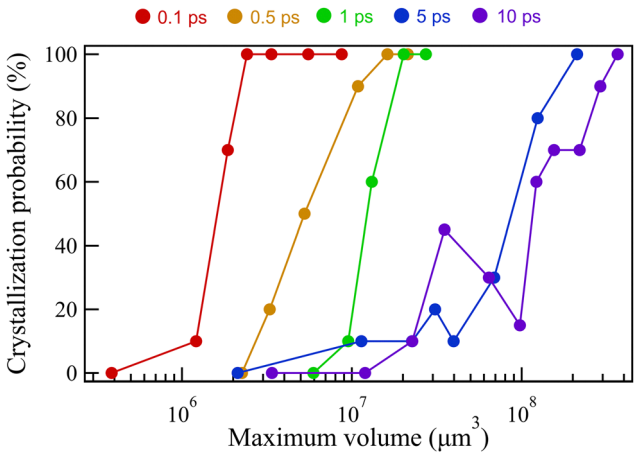

Fig. 6 Crystallization probability as a function of the maximum volume of the cavitation bubble. The maximum volume was extracted from the fitting curves in Fig. S8 (ESI†).

viewpoint of cavitation bubbles. In a previous study, we found that the probability of urea crystallization from supersaturated aqueous solutions could be scaled by the cube of the maximum radius of a cavitation bubble, which was measured by observing the axial direction of the laser irradiation. To investigate the impact of the cavitation bubbles on the crystallization of AcOK, we plotted the crystallization probability as a function of the maximum volume of the cavitation bubbles, as shown in Fig. 6. In this work, the volume of the cavitation bubble was approximated by $4\pi/3 \times (\text{length}/2) \times (\text{width}/2)^2$, which takes into account the elongated shape of cavitation bubbles (Fig. 3 and 4). The cavitation bubbles typically reached their maximum volume when the width reached the maximum value. The dependence of the maximum volume of the cavitation bubbles on the laser energy and pulse duration is shown in Fig. S8 (ESI†). Although larger cavitation bubbles may potentially provide higher concentration increase due to faster bubble growth velocity,[53] the overall trend shown in Fig. 6 indicates that shorter laser pulses can induce crystal nucleation, even with smaller cavitation bubbles. For instance, the maximum volume of the cavitation bubble at the laser energy where the crystallization starts to occur is estimated to be 1.2×10^6 μm^3 for the 0.1-ps laser pulse (10% at E = 5 μJ per pulse), 3.3×10^6 μm^3 for the 0.5-ps laser pulse (20% at E = 10 μJ per pulse), 9.5×10^6 μm^3 for the 1-ps laser pulse (10% at E = 22 μJ per pulse), 11×10^6 μm^3 for the 5-ps laser pulse (10% at E = 25 μJ per pulse), and 23×10^6 μm^3 for the 10-ps laser pulse (10% at E = 45 μJ per pulse). In addition, the maximum volume of cavitation bubbles that reached 100% crystallization probability is estimated to be 2.4×10^6 μm^3 for the 0.1-ps laser pulse (E = 10 μJ per pulse), 16×10^6 μm^3 for the 0.5-ps laser pulse (E = 45 μJ per pulse), 20×10^6 μm^3 for the 1-ps laser pulse (E = 45 μJ per pulse), 210×10^6 μm^3 for the 5-ps laser pulse (E = 210 μJ per pulse), and 370×10^6 μm^3 for the 10-ps laser pulse (E = 300 μJ per pulse). This trend can be attributed to the difference in the temperature elevation among the pulse durations. Temperature elevation in the AcOK solution led to a decrease in supersaturation,[68] whereas laser irradiation was accompanied by temperature elevation. Theoretically, an increase in laser energy results in a higher temperature elevation because the absorbed energy increases. As for the pulse duration dependence, several studies have reported that longer laser pulses tend to induce a higher temperature elevation in supersaturated solutions of some organic chemical compounds.[40,54] In the case of longer laser pulses (*e.g.*, picosecond laser), the electron excitation and relaxation potentially recur within a pulse duration, which may result in large heat generation that causes significant temperature elevation around the laser focus.[69] By contrast, in the case of shorter laser pulses (*e.g.*, femtosecond laser), the generated heat during the process of rapid electron excitation and relaxation is preferentially converted into thermoelastic pressure that induces a shockwave.[69] The generation of a shockwave suppresses temperature elevation around the laser focus.[69] Therefore, because of the smaller heat effects, the shorter laser pulses can exhibit higher crystallization probability even with generation of smaller cavitation bubbles. The experimental result that the crystallization probability for the 5- and 10-ps laser pulses decreased at a certain

laser energy (Fig. 3b, 5-ps laser pulse: 50 μJ per pulse to 60 μJ per pulse, 10-ps laser pulse: 60 μJ per pulse to 120 μJ per pulse) may also be attributed to larger temperature elevation with longer laser pulse that disturbs the positive effect of concentration increase on the crystal nucleation. Indeed, the negative impact of temperature elevation on crystallization has also been reported in previous studies targeting urea and sodium acetate solutions, where shorter laser pulses exhibited a higher crystallization probability with smaller cavitation bubbles.[40,54]

It should be noted that shorter laser pulses do not always result in a higher crystallization probability. For instance, in the case of glacial acetic acid and ice, a few picosecond laser pulses (*e.g.*, 5-ps laser pulses) could provide 100% crystallization probability, while ~0.1-ps laser pulse exhibited significantly smaller crystallization probability (*e.g.*, 40% at a maximum) even after systematic screening of laser energy.[37,39] Indeed, the size of cavitation bubbles induced by femtosecond laser pulses (*e.g.*, 0.1-ps laser pulses) often immediately saturates with laser energy (see Fig. 5), suggesting that the driving force for crystallization given by cavitation bubbles may not be sufficient for the crystallization of these compounds. On the other hand, cavitation bubbles produced by several picosecond laser pulses (*e.g.*, 5-ps laser pulses) often continue to increase with laser energy (see Fig. 5). Our experimental finding that the 5- and 10-ps laser pulses eventually provide 100% crystallization probability at significantly higher laser energy (≥200 μJ per pulse) (Fig. 2b) may indicate that the effect of cavitation bubble generation (positive factor) is relatively larger than that of temperature elevation (negative factor) eventually. Accordingly, it may be interpreted that the pulse duration is trivial and that simply setting a larger laser energy is sufficient to efficiently trigger crystal nucleation. However, it should be noted that the crystallization probability of some materials does not saturate at 100% with respect to the laser energy, as exemplified by the case of ice where crystallization probability with a 10-ns laser pulses saturates at 60%.[39] In addition, polymorphs are sensitive to the concentration and temperature in laser irradiation,[40] and thus, a higher laser energy may not guarantee the desired crystal polymorphs. Overall, it can be concluded that the precise regulation of the positive (*e.g.*, generation of cavitation bubbles) and negative effects (*e.g.*, temperature elevation) of laser irradiation is crucial for achieving sophisticated control of metastable crystallization *via* laser ablation.

Conclusions

This study demonstrated the crystallization of a metastable phase of potassium acetate (AcOK) *via* ultrashort laser ablation. By systematically varying the laser pulse durations and energies, we revealed that shorter pulses (*e.g.*, 0.1-ps laser pulses) significantly enhance the probability of metastable-phase crystallization. Cavitation bubbles, a possible trigger for laser ablation-induced crystallization, were also investigated under various laser parameters, revealing that shorter laser pulses can provide a higher crystallization probability with smaller cavitation bubbles. This is because the temperature elevation, which leads to a decrease in the supersaturation of the AcOK solution, is possibly suppressed by irradiation with shorter laser pulses. Our findings highlight that the precise regulation of laser-induced effects, particularly the interplay between the cavitation bubble behavior (positive factors for nucleation) and temperature elevation (negative factors for nucleation), is essential for the efficient preparation of the metastable phase *via* laser ablation. By offering insights into the mechanisms driving polymorphic control, this study paves the way for novel applications in pharmaceuticals, advanced materials, and chemical engineering, where precise polymorph selection is of paramount importance. We also expect that further quantitative analyses of the concentration and temperature dynamics upon laser irradiation using advanced techniques (*e.g.*, fluorescence imaging[52,70]) may contribute to the establishment of sophisticated guiding principles.

Author contributions

Hozumi Takahashi: conceptualization, methodology, investigation, formal analysis, writing – original draft, writing – review & editing, funding acquisition. Hiroshi Y. Yoshikawa: conceptualization, writing – review & editing, funding acquisition.

Conflicts of interest

There are no conflicts to declare.

Data availability

The data supporting the results presented in this article are available either within the article or included as part of the ESI.†

Acknowledgements

This work was partially supported by grants from the Japan Science and Technology Agency (JST) through the ACT-X Program (No. JPMJAX23DC to HT) and Japan Society for the Promotion of Science (JSPS) KAKENHI (JP24KK0106, JP24H01138, JP23K18576, and JP22H00302 to HYY, JP25K17959 to HT). We extend our gratitude to the Iketani Science and Technology Foundation (HT), Kurita Water and Environment Foundation (HT), Amada Foundation (HYY), Asahi Glass Foundation (HYY), Natakani Foundation (HYY), Takeda Science Foundation (HYY), and Murata Science and Education Foundation (HYY) for their assistance.

References

1 H. G. Brittain, *Drugs Pharm. Sci.*, 1999, **95**, 183–226.
2 S. L. Morissette, Ö. Almarsson, M. L. Peterson, J. F. Remenar, M. J. Read, A. V. Lemmo, S. Ellis, M. J. Cima and C. R. Gardner, *Adv. Drug Delivery Rev.*, 2004, **56**, 275–300.
3 Y. Diao, K. M. Lenn, W.-Y. Lee, M. A. Blood-Forsythe, J. Xu, Y. Mao, Y. Kim, J. A. Reinspach, S. Park, A. Aspuru-Guzik,

G. Xue, P. Clancy, Z. Bao and S. C. B. Mannsfeld, *J. Am. Chem. Soc.*, 2014, **136**, 17046–17057.
4 B. A. Nogueira, C. Castiglioni and R. Fausto, *Commun. Chem.*, 2020, **3**, 34.
5 G. Liu, R. Gou, H. Li and C. Zhang, *Cryst. Growth Des.*, 2018, **18**, 4174–4186.
6 D. K. Bučar, R. W. Lancaster and J. Bernstein, *Angew. Chem., Int. Ed.*, 2015, **54**, 6972–6993.
7 A. J. Alexander and P. J. Camp, *J. Chem. Phys.*, 2019, **150**, 040901.
8 T. Sugiyama and S.-F. Wang, *J. Photochem. Photobiol., C*, 2022, **52**, 100530.
9 N. Nagalingam, A. Raghunathan, V. Korede, C. Poelma, C. S. Smith, R. Hartkamp, J. T. Padding and H. B. Eral, *Phys. Rev. Lett.*, 2023, **131**, 124001.
10 B. A. Garetz, J. E. Aber, N. L. Goddard, R. G. Young and A. S. Myerson, *Phys. Rev. Lett.*, 1996, **77**, 3475–3476.
11 C. Duffus, P. J. Camp and A. J. Alexander, *J. Am. Chem. Soc.*, 2009, **131**, 11676–11677.
12 B. A. Garetz, J. Matic and A. S. Myerson, *Phys. Rev. Lett.*, 2002, **89**, 175501.
13 X. Sun, B. A. Garetz and A. S. Myerson, *Cryst. Growth Des.*, 2008, **8**, 1720–1722.
14 A. Ikni, B. Clair, P. Scouflaire, S. Veesler, J.-M. Gillet, N. El Hassan, F. Dumas and A. Spasojevic-de Bire, *Cryst. Growth Des.*, 2014, **14**, 3286–3299.
15 W. Li, A. Ikni, P. Scouflaire, X. Shi, N. El Hassan, P. Gemeiner, J.-M. Gillet and A. Spasojevic-de Bire, *Cryst. Growth Des.*, 2016, **16**, 2514–2526.
16 T. Sugiyama, T. Adachi and H. Masuhara, *Chem. Lett.*, 2007, **36**, 1480–1481.
17 T. Sugiyama, K.-i Yuyama and H. Masuhara, *Acc. Chem. Res.*, 2012, **45**, 1946–1954.
18 H. Takahashi, H. Y. Yoshikawa and T. Sugiyama, *J. Photochem. Photobiol., A*, 2024, **456**, 115845.
19 K.-i Yuyama, T. Rungsimanon, T. Sugiyama and H. Masuhara, *Cryst. Growth Des.*, 2012, **12**, 2427–2434.
20 C.-S. Wu, P.-Y. Hsieh, K.-I. Yuyama, H. Masuhara and T. Sugiyama, *Cryst. Growth Des.*, 2018, **18**, 5417–5425.
21 C.-S. Wu, H. Y. Yoshikawa and T. Sugiyama, *Jpn. J. Appl. Phys.*, 2020, **59**, SIIH02.
22 T.-W. Shih, C.-L. Hsu, L.-Y. Chen, Y.-C. Huang, C.-J. Chen, Y. Inoue and T. Sugiyama, *Cryst. Growth Des.*, 2021, **21**, 6913–6923.
23 W.-C. Wang, S.-F. Wang and T. Sugiyama, *J. Chin. Chem. Soc.*, 2022, **69**, 200–210.
24 A.-C. Cheng, H. Niinomi, T. Omatsu, S. Ishida, K. Sasaki and T. Sugiyama, *J. Phys. Chem. Lett.*, 2020, **11**, 4422–4426.
25 K. Toyoda, H.-T. Su, K. Miyamoto, T. Sugiyama and T. Omatsu, *Optica*, 2023, **10**, 332–338.
26 A.-C. Cheng, C. Pin, Y. Sunaba, T. Sugiyama and K. Sasaki, *Small*, 2024, **20**, 2312174.
27 A.-C. Cheng, C. Pin, T. Sugiyama and K. Sasaki, *J. Phys. Chem. C*, 2024, **128**, 4314–4320.
28 T. Sugiyama, T.-M. Lin, H.-T. Su, A.-C. Cheng and K. Sasaki, *J. Chem. Phys.*, 2024, **160**, 064502.
29 H.-T. Su, H. Niinomi, A.-C. Cheng, Y. Y. Tanaka, K. Sasaki and T. Sugiyama, *Cell Rep. Phys. Sci.*, 2024, **5**, 102310.
30 H. Niinomi, K. Gotoh, N. Takano, M. Tagawa, I. Morita, A. Onuma, H. Y. Yoshikawa, R. Kawamura, T. Oshikiri and M. Nakagawa, *J. Phys. Chem. Lett.*, 2024, **15**, 1564–1571.
31 H. Y. Yoshikawa, R. Murai, H. Adachi, S. Sugiyama, M. Maruyama, Y. Takahashi, K. Takano, H. Matsumura, T. Inoue, S. Murakami, H. Masuhara and Y. Mori, *Chem. Soc. Rev.*, 2014, **43**, 2147–2158.
32 H. Y. Yoshikawa, Y. Hosokawa, R. Murai, G. Sazaki, T. Kitatani, H. Adachi, T. Inoue, H. Matsumura, K. Takano and S. Murakami, *Cryst. Growth Des.*, 2012, **12**, 4334–4339.
33 Y. Tominaga, M. Maruyama, M. Yoshimura, H. Koizumi, M. Tachibana, S. Sugiyama, H. Adachi, K. Tsukamoto, H. Matsumura, K. Takano, S. Murakami, T. Inoue, H. Y. Yoshikawa and Y. Mori, *Nat. Photonics*, 2016, **10**, 723–726.
34 D. Suzuki, S. Nakabayashi and H. Y. Yoshikawa, *Cryst. Growth Des.*, 2018, **18**, 4829–4833.
35 C. S. Wu, J. Ikeyama, S. Nakabayashi, T. Sugiyama and H. Y. Yoshikawa, *J. Phys. Chem. C*, 2019, **123**, 24919–24926.
36 H. Takahashi, M. Yamaji, J. Ikeyama, M. Nakajima, H. Kitahara, S. Tetsukawa, N. Kobayashi, M. Maruyama, T. Sugiyama, S. Okada, Y. Mori, S. Nakabayashi, M. Yoshimura and H. Y. Yoshikawa, *J. Phys. Chem. C*, 2021, **125**, 8391–8397.
37 H. Takahashi, T. Sugiyama, S. Nakabayashi and H. Y. Yoshikawa, *Appl. Phys. Express*, 2021, **14**, 045503.
38 H. Takahashi, M. Shiraiwa, V. K. Mag-usara, R. Dai, V. C. Agulto, K. Kato, M. Nakajima, M. Yamaji, S. Nakabayashi, M. Maruyama, Y. Mori, M. Yoshimura and H. Y. Yoshikawa, *J. Phys. Chem. C*, 2023, **127**, 14005–14012.
39 H. Takahashi, T. Kono, K. Sawada, S. Kumano, Y. Tsuri, M. Maruyama, M. Yoshimura, D. Takahashi, Y. Kawamura, M. Uemura, S. Nakabayashi, Y. Mori, Y. Hosokawa and H. Y. Yoshikawa, *J. Phys. Chem. Lett.*, 2023, **14**, 4394–4402.
40 H. Takahashi, Y. Takaoka, S. Ebihara, Y. Tsuri, M. Maruyama, M. Yoshimura, Y. Mori and H. Y. Yoshikawa, *J. Phys. Chem. C*, 2024, **128**, 11046–11053.
41 H. Takahashi, Y. Yoshimura, R. Murai, R. Kawamura, M. Maruyama, M. Yoshimura, Y. Mori and H. Y. Yoshikawa, *J. Phys. Chem. Lett.*, 2024, **15**, 180–186.
42 H. Takahashi and H. Y. Yoshikawa, *J. Phys. Chem. C*, 2025, **129**, 8346–8353.
43 K. Ikeda, M. Maruyama, Y. Takahashi, Y. Mori, H. Y. Yoshikawa, S. Okada, H. Adachi, S. Sugiyama, K. Takano and S. Murakami, *Appl. Phys. Express*, 2015, **8**, 045501.
44 Y. Tsuri, M. Maruyama, R. Fujimoto, S. Okada, H. Adachi, H. Y. Yoshikawa, K. Takano, S. Murakami, H. Matsumura and T. Inoue, *Appl. Phys. Express*, 2018, **12**, 015507.
45 S. Wang, S. Wang, L. Jiang, M. Wang, Y. Wei, J. Sun, S. Zhan, X. Li and L. Qu, *Cryst. Growth Des.*, 2019, **19**, 3265–3271.
46 J. Yu, J. Yan and L. Jiang, *Cryst. Growth Des.*, 2021, **21**, 3202–3210.
47 N. Kaneniwa, M. Otsuka and T. Hayashi, *Chem. Pharm. Bull.*, 1985, **33**, 3447–3455.

48 K. Nakamura, Y. Hosokawa and H. Masuhara, *Cryst. Growth Des.*, 2007, **7**, 885–889.
49 H. Y. Yoshikawa, R. Murai, S. Maki, T. Kitatani, S. Sugiyama, G. Sazaki, H. Adachi, T. Inoue, H. Matsumura and K. Takano, *Appl. Phys. A: Mater. Sci. Process.*, 2008, **93**, 911–915.
50 H. Y. Yoshikawa, R. Murai, S. Sugiyama, G. Sazaki, T. Kitatani, Y. Takahashi, H. Adachi, H. Matsumura, S. Murakami, T. Inoue, K. Takano and Y. Mori, *J. Cryst. Growth*, 2009, **311**, 956–959.
51 A. Soare, R. Dijkink, M. R. Pascual, C. Sun, P. W. Cains, D. Lohse, A. I. Stankiewicz and H. J. Kramer, *Cryst. Growth Des.*, 2011, **11**, 2311–2316.
52 N. Iefuji, R. Murai, M. Maruyama, Y. Takahashi, S. Sugiyama, H. Adachi, H. Matsumura, S. Murakami, T. Inoue, Y. Mori, Y. Koga, K. Takano and S. Kanaya, *J. Cryst. Growth*, 2011, **318**, 741–744.
53 N. Hidman, G. Sardina, D. Maggiolo, H. Ström and S. Sasic, *Cryst. Growth Des.*, 2020, **20**, 7276–7290.
54 Y. Tsuri, M. Maruyama, K. Tsukamoto, H. Adachi, K. Takano, S. Usami, M. Imanishi, M. Yoshimura, H. Y. Yoshikawa and Y. Mori, *Appl. Phys. A: Mater. Sci. Process.*, 2022, **128**, 1–7.
55 P. Kalle, S. I. Bezzubov, E. V. Latipov and A. V. Churakov, *Inorg. Chem.*, 2025, **64**, 2146–2153.
56 D. B. Lawrence, T. T. Cai and D. Anirban, *Stat. Sci.*, 2001, **16**, 101–133.
57 A. Heisterkamp, T. Ripken, T. Mamom, W. Drommer, H. Welling, W. Ertmer and H. Lubatschowski, *Appl. Phys. B: Lasers Opt.*, 2002, **74**, 419–425.
58 R. Murai, H. Y. Yoshikawa, H. Hasenaka, Y. Takahashi, M. Maruyama, S. Sugiyama, H. Adachi, K. Takano, H. Matsumura and S. Murakami, *Chem. Phys. Lett.*, 2011, **510**, 139–142.
59 L. Geiger, I. Howard, N. MacKinnon, A. Forbes and J. G. Korvink, *Cryst. Growth Des.*, 2024, **24**, 3589–3594.
60 Y. Mori, M. Maruyama, Y. Takahashi, K. Ikeda, S. Fukukita, H. Y. Yoshikawa, S. Okada, H. Adachi, S. Sugiyama and K. Takano, *Appl. Phys. Express*, 2015, **8**, 065501.
61 Y. Mori, M. Maruyama, Y. Takahashi, H. Y. Yoshikawa, S. Okada, H. Adachi, S. Sugiyama, K. Takano, S. Murakami and H. Matsumura, *Appl. Phys. Express*, 2017, **10**, 025501.
62 Y. Tsuri, N. Inaoka, M. Maruyama, K. Tsukamoto, H. Adachi, H. Y. Yoshikawa, K. Takano, M. Imanishi, M. Yoshimura and Y. Mori, *J. Cryst. Growth*, 2021, **557**, 125994.
63 A. Nishigaki, M. Maruyama, S.-I. Tanaka, H. Y. Yoshikawa, M. Imanishi, M. Yoshimura, Y. Mori and K. Takano, *Crystals*, 2022, **12**, 1104.
64 F. Potemkin, E. Mareev, A. Podshivalov and V. Gordienko, *New J. Phys.*, 2015, **17**, 053010.
65 F. Potemkin and E. Mareev, *Laser Phys. Lett.*, 2014, **12**, 015405.
66 J. Noack, D. X. Hammer, G. D. Noojin, B. A. Rockwell and A. Vogel, *J. Appl. Phys.*, 1998, **83**, 7488–7495.
67 A. Vogel, J. Noack, K. Nahen, D. Theisen, S. Busch, U. Parlitz, D. Hammer, G. Noojin, B. Rockwell and R. Birngruber, *Appl. Phys. B: Lasers Opt.*, 1999, **68**, 271–280.
68 R. Abe, *Tokyo Kagaku Kaishi*, 1911, **32**, 979–985.
69 Y. Hosokawa, *Jpn. J. Appl. Phys.*, 2019, **58**, 110102.
70 P. A. Quinto-Su, M. Suzuki and C.-D. Ohl, *Sci. Rep.*, 2014, **4**, 5445.

